GEOPHYSICS, VOL. 65, NO. 4 (JULY–AUGUST 2000); P. 1080–1092, 15 FIGS., 1 TABLE.

A model for seismic velocity and attenuation in petroleum source rocks

José M. Carcione*

ABSTRACT

Petroleum source rock is modeled as a viscoelastic transversely isotropic medium composed of illite/ smectite and organic matter. The wave velocities and attenuation of petroleum source rocks are obtained as a function of excess pore pressure, initial kerogen content, and water saturation. The model generalizes a previous approach based on a pure elastic formulation of Backus averaging and introduces the pressure effect and the presence of fluids (oil and water). The model allows the simulation of different maturation levels induced by pore-pressure changes caused by the conversion of kerogen to oil. The higher the oil saturation, the higher the maturation level. Assuming that the source rock has a very low permeability, the excess pore pressure can be calculated as a function of the conversion factor. Then the bulk modulus and density of the kerogen/oil mixture are obtained with the Kuster and Toksöz model, assuming that oil is the inclusion in a kerogen matrix. Finally, Backus averaging of this mixture with the illite/smectite layers gives the complex stiffnesses of the transversely isotropic and anelastic medium.

Computed P- and S-velocities and quality factors parallel to bedding are higher than those normal to bedding, with attenuation anisotropy higher than stiffness anisotropy. In particular, for the North Sea Kimmeridge Shale and at maximum anisotropy, P and S parallel velocities are approximately 0.7 km/s higher than the corresponding P and S normal velocities. The maximum attenuation and stiffness anisotropies are obtained for 18% and 30% volumetric kerogen content, respectively. Both velocities and quality factors decrease with increasing kerogen content at a given pore pressure. The decrease in wave velocity is 2 km/s for P-waves and 1 km/s for S-waves when kerogen increases from zero to 100%. Moreover, anisotropy increases and velocities decrease with increasing pore pressure, i.e., with higher kerogen-to-oil conversion. Finally, the presence of water affects the normal-bedding velocity, i.e., higher water saturation implies lower velocities.

INTRODUCTION

The aim of this work is to obtain a model for source rocks relating seismic anisotropy (in velocity and attenuation) to kerogen content, pore pressure, and water saturation. Recent petrophysical analyses of petroleum source rocks (Vernik and Nur, 1992; Vernik, 1994; Vernik and Landis, 1996) indicate that the observed strong-velocity anisotropy can be associated with the presence of organic matter and its distribution in the rock matrix. Most hydrocarbon source rocks are laminated structures composed of organic matter (kerogen and oil) and illite layers. When the seismic wavelength is much larger than the thickness of the single layers, the finely layered medium behaves as a homogeneous, transversely isotropic material whose stiffnesses can be obtained by using Backus averaging technique (Schoenberg and Muir, 1989). Assuming that the illite and the organic material are attenuating media, a generalization of the averaging technique to the dissipative case gives not only the wave velocities (Vernik and Nur, 1992; Vernik, 1994) but also the dissipation factors as a function of organic matter and propagation direction (Carcione, 1992).

The maturation level of source rocks can be associated with oil generation and overpressuring (e.g., Meissner, 1978). If the conversion rate is more rapid than the rate of volume loss by fluid flow, excess pore pressure is generated. Berg and Gangi (1999) developed a simple relation to calculate the excess pore pressure caused by kerogen converting to oil. On the basis of this relation, the model assumptions and steps can be summarized in the following: (1) source rocks are made of clay layers and hydrocarbons (kerogen plus oil); (2) the amount of generated oil depends on the degree of maturation and is

Manuscript received by the Editor January 27, 1998; revised manuscript received October 21, 1999.
*Istituto Nazionale di Oceanografia e di Geofisica Sperimentale, Borgo Grotta Gigante 42c, 34010 Sgonico, Trieste, Italy. E-mail: jcarcione@ogs.trieste.it.

related to the excess pore pressure (Berg and Gangi, 1999); (3) the Kuster and Toksöz (1974) theory is used to calculate the acoustic properties of kerogen with oil inclusions; (4) Backus averaging, generalized to the dissipative case, is used to obtain the effective acoustic properties of the (viscoelastic and transversely isotropic) source rock; and (5) the phase velocities and quality factors versus excess pore pressure are obtained with a plane-wave analysis.

A typical situation in the North Sea source rocks is represented by the Kimmeridge Shale, a source rock from the Draupne Formation, with a maximum thickness of nearly 200 m, overlain by high-velocity chalk. The observed velocity contrast and thickness make the Kimmeridge an easily identified seismic unit. *P*-wave impedance contrasts between the overlying chalk and the hydrocarbon source rock (normal and parallel to the bedding plane) are calculated as a function of organic content and pore pressure.

COMPOSITE MODEL OF THE SOURCE ROCK

Following Vernik and Nur (1992), we assume that the immature rock is a two-layer composite made of illite and kerogen, with no additional pore fluid. We consider illite transversely isotropic, kerogen isotropic, and both materials viscoelastic. Using Backus averaging gives a transversely isotropic equivalent medium described by five complex effective stiffnesses c^*_{IJ}, where

$$\begin{aligned} c^*_{11} &= \langle c_{11} - c_{13}^2 c_{33}^{-1}\rangle + \langle c_{33}^{-1}\rangle^{-1}\langle c_{33}^{-1} c_{13}\rangle^2,\\ c^*_{33} &= \langle c_{33}^{-1}\rangle^{-1},\\ c^*_{13} &= \langle c_{33}^{-1}\rangle^{-1}\langle c_{33}^{-1} c_{13}\rangle,\\ c^*_{55} &= \langle c_{55}^{-1}\rangle^{-1},\\ c^*_{66} &= \langle c_{66}\rangle, \end{aligned} \tag{1}$$

with c_{IJ} the complex stiffnesses corresponding to the single constituents (illite and kerogen). Equations (1) are a generalization of the averaging equations developed by Schoenberg and Muir (1989) to the lossy case, using the correspondence principle (e.g., Ben-Menahem and Singh, 1981; Carcione, 1992). Denoting the proportion of volumetric kerogen content by K, the weighted average of any physical quantity a in equation (1) is defined as

$$\langle a\rangle = (1-\mathrm{K})a_i + \mathrm{K}a_k, \tag{2}$$

where the subscripts i and k indicate illite and kerogen.

For illite, we assume that the mean stress (i.e., the trace of the stress tensor) depends only on the dilatational complex modulus M_1. Moreover, the deviatoric stress components depend solely on the shear complex modulus, denoted by M_2 (Carcione et al., 1998). The complex stiffnesses for such transversely isotropic and viscoelastic medium are given by

$$c_{I(I)} = \hat{c}_{I(I)} - D + BM_1 + \frac{4}{3}GM_2, \qquad I = 1,2,3, \tag{3}$$

$$c_{IJ} = \hat{c}_{IJ} - D + BM_1 + 2G\left(1 - \frac{1}{3}M_2\right), \qquad I, J = 1,2,3; \quad I \neq J, \tag{4}$$

$$c_{55} = \hat{c}_{55}M_2, \qquad c_{66} = \hat{c}_{66} + G(M_2 - 1), \tag{5}$$

with

$$B = D - \frac{4}{3}G \tag{6}$$

and

$$D = \frac{1}{3}(2\hat{c}_{11} + \hat{c}_{33}), \qquad G = \frac{1}{3}(2\hat{c}_{55} + \hat{c}_{66}), \tag{7}$$

where $\hat{c}_{IJ}$ are the unrelaxed (high-frequency limit) elastic constants (e.g., Carcione et al., 1998).

As stated by Vernik and Nur (1992), the organic material can be viewed as an amorphous (isotropic) substance subject to liquefaction with increasing temperature and pressure. Each layer of kerogen is described by the complex Lamé parameters given by Carcione et al. (1998),

$$\begin{aligned} c_{13} &= \rho_k\left(V_{11}^2 - \frac{4}{3}V_{55}^2\right)M_1 - \frac{2}{3}\rho_k V_{55}^2 M_2,\\ \text{and}\\ c_{55} &= \rho_k V_{55}^2 M_2, \end{aligned} \tag{8}$$

where V_{11} and V_{55} are the elastic high-frequency limit compressional and shear velocities, and ρ_k is the density [note that in Carcione (1992), the elastic limit corresponds to the relaxed moduli]. Because the medium is isotropic, $c_{11} = c_{33} = c_{13} + 2c_{55}$ and $c_{66} = c_{55}$.

Equations (3) through (6) and (8) give the stiffnesses of illite and kerogen as a function of density, elastic constants, and complex moduli, which define the amount of attenuation. The following attenuation model assumes a single standard linear solid element (Ben-Menahem and Singh, 1981) describing each anelastic deformation mode (identified by the index ν) whose (dimensionless) complex moduli can be expressed as

$$M_\nu(\omega) = \frac{\sqrt{Q_\nu^2+1} - 1 + i\omega Q_\nu \tau_0}{\sqrt{Q_\nu^2+1} + 1 + i\omega Q_\nu \tau_0}, \qquad \nu = 1,2, \tag{9}$$

where ω is the angular frequency. The quality factor associated with each modulus is equal to the real part of M_ν divided by its imaginary part. At $\omega_0 = 1/\tau_0$, the associated quality factor curve has its highest value Q_ν. For a given angular frequency ω, we take $\tau_0\omega = 1$ because we are intererested in the anisotropic properties of attenuation, and therefore the frequency dependence is irrelevant. The high-frequency limit corresponds to the elastic case with $M_\nu \to 1$.

The volumetric kerogen content (in percentage) can be transformed to total organic carbon (TOC, weight percent) by using

$$\mathrm{TOC} = 0.75\rho_k\langle\rho\rangle^{-1}\mathrm{K}, \tag{10}$$

where $\langle\rho\rangle$ is the density of the source rock and 0.75 is a constant relating TOC to kerogen weight percent (Vernik and Nur, 1992). Using equation (2), we get

$$\mathrm{TOC} = \frac{0.75\rho_k \mathrm{K}}{\rho_i - \mathrm{K}(\rho_i - \rho_k)}. \tag{11}$$

PHASE VELOCITY, ATTENUATION, AND QUALITY FACTOR

Substitution of the stress-strain relation for plane waves into the equations of momentum conservation gives the complex Christoffel equation (Carcione et al., 1998). The eigenvalues of

the Christoffel matrix are related closely to the complex velocities of the three propagating modes—the quasi-compressional wave, denoted by qP, the quasi-shear wave, denoted by qS, and the pure shear wave, denoted by S (Carcione et al., 1998). For homogeneous viscoelastic waves, the complex velocity V is a fundamental quantity because it determines uniquely both the attenuation and the quality factors. For instance, the three waves propagating in the (x, z)-plane of a transversely isotropic medium, where the z-axis is directed along the symmetry axis, have the following velocities along the coordinate axes:

$$\begin{aligned} V_{qS}(0) &= V_{qS}(90) = \sqrt{c^*_{55}/\rho}, \\ V_{qP}(0) &= \sqrt{c^*_{33}/\rho}, \qquad V_{qP}(90) = \sqrt{c^*_{11}/\rho}, \\ V_S(0) &= \sqrt{c^*_{55}/\rho}, \qquad V_S(90) = \sqrt{c^*_{66}/\rho}, \end{aligned} \tag{12}$$

where 0 corresponds to the z-axis and 90 to the x-axis.

The magnitude of the attenuation vector is given by

$$\alpha = -\omega\,\mathrm{Im}(V^{-1}) \tag{13}$$

and the quality factor by

$$Q = \frac{\mathrm{Re}(V^2)}{\mathrm{Im}(V^2)}, \tag{14}$$

where Re and Im denote real and imaginary parts. Note that V and Q depend on the unrelaxed elasticities, the complex moduli, and the propagation direction.

Attenuation and Q factor are related by

$$\alpha = \omega\big(\sqrt{Q^2+1} - Q\big)\mathrm{Re}(V^{-1}). \tag{15}$$

For low-loss solids, where $Q \gg 1$, a Taylor expansion yields

$$\alpha \cong \frac{\omega}{2Q}\,\mathrm{Re}(V^{-1}) = \frac{\pi f}{Q V_{ph}}, \tag{16}$$

where f is the frequency and V_{ph} is the phase velocity given by

$$V_{ph} = [\mathrm{Re}(V^{-1})]^{-1}. \tag{17}$$

Equation (16) is the well-known relation between attenuation and quality factor (e.g., Toksöz and Johnston, 1981).

On the other hand, the anisotropy parameters, introduced by Thomsen (1986), can be redefined as

$$\begin{aligned} \epsilon_R &= \frac{c^*_{11\,\mathrm{R}} - c^*_{33\,\mathrm{R}}}{2c^*_{33\,\mathrm{R}}}, \qquad \gamma_R = \frac{c^*_{66\,\mathrm{R}} - c^*_{55\,\mathrm{R}}}{2c^*_{55\,\mathrm{R}}}, \\ \delta_R &= \frac{\big(c^*_{13\,\mathrm{R}} + c^*_{55\,\mathrm{R}}\big)^2 - \big(c^*_{33\,\mathrm{R}} - c^*_{55\,\mathrm{R}}\big)^2}{2c^*_{33\,\mathrm{R}}\big(c^*_{33\,\mathrm{R}} - c^*_{55\,\mathrm{R}}\big)}, \end{aligned} \tag{18}$$

where the subindex R denotes the real part. Equivalent parameters to ϵ_R and γ_R, quantifying the anisotropic attenuation, can be defined as

$$\begin{aligned} \epsilon_I &= \frac{Q_{11} - Q_{33}}{2Q_{33}} = \frac{1}{2}\left[\frac{c^*_{33\,\mathrm{Im}}}{c^*_{11\,\mathrm{Im}}}(2\epsilon_R + 1) - 1\right], \\ \gamma_I &= \frac{Q_{66} - Q_{55}}{2Q_{55}} = \frac{1}{2}\left[\frac{c^*_{55\,\mathrm{Im}}}{c^*_{66\,\mathrm{Im}}}(2\gamma_R + 1) - 1\right], \end{aligned} \tag{19}$$

where

$$Q_{IJ} = \frac{c^*_{IJ\,\mathrm{R}}}{c^*_{IJ\,\mathrm{Im}}} \tag{20}$$

are the quality factors along the "crystal" axes and the subindex I denotes the imaginary part. Note that, for instance, when $c^*_{11\,\mathrm{Im}} = c^*_{33\,\mathrm{Im}}$, then $\epsilon_I = \epsilon_R$, which does not imply isotropic attenuation.

EXAMPLE

The material properties of the different media are given in Table 1, where $V_{IJ} = \sqrt{\hat{c}_{IJ}/\rho}$ are the elastic (unrelaxed) velocities (here, ρ denotes the density of a single constituent), and ϵ, γ, and δ denote the unrelaxed anisotropic coefficients introduced by Thomsen (1986). The properties of illite and immature kerogen are obtained by fitting experimental data for the Kimmeridge Shale. The clay in this shale is represented predominantly by illite and kaolinite, with the volume percentage of smectite varying from 0% to 10% of the rock. The low velocities for illite take into account a fluid-softening effect by hydration of the smectite, and the values of the quality factors are based on in situ measurements for shale, at a depth of 1700 m (Hauge, 1981). We assume that the properties of the source rock depend on the maturation stage (Vernik, 1994). From normal pore pressure (immature rock) to high pore pressure (mature rock), the kerogen is transformed gradually into oil with the properties indicated in the table. Mature rocks have a more plastic behavior because of their higher hydrocarbon content (HC), and therefore, anelastic effects increase in this context (Johnston, 1987). This process is enhanced by smectite/illite transformation, which generates free water. The presence of a more compliant and liquidlike medium (kerogen + oil) triggers new attenuation mechanisms. Moreover, dissipation also is enhanced by the creation of microcracks by overpressuring induced by hydrocarbon generation (Vernik, 1992). All these mechanisms are contained in the dilatational quality factor Q_1, assigned to oil in Table 1. In this context, we may consider that Q_1 is a free parameter for adjusting the theory to the experimental data. The value given in Table 1 is assumed because no experimental attenuation data are available on source rocks.

Table 1. Material properties.

Medium	V_{11} (km/s)	V_{33} (km/s)	V_{55} (km/s)	V_{66} (km/s)	V_{13} (km/s)	ϵ	γ	δ	ρ (g/cm^{-3})	Q_1	Q_2
Illite*	4.7	4.36	2.46	2.77	2.43	0.08	0.1	−0.05	2.7	270	200
Kerogen*	2.6	2.6	1.2	1.2	1.97	0	0	0	1.4	30	20
Oil†	0.73	0.73	0	0	0.73	0	0	0	0.9	10	—

*Vernik (1994).
†Oil/bitumen (McCain, 1984).

Immature source rock

Kerogen in the Kimmeridge Shale is associated mostly with source type II organic matter (e.g., see Vernik, 1994). Therefore, the rock is in an early maturation stage, with few free hydrocarbons. Total organic carbon can be expressed as a function of rock density from the empirical relations of Vernik and Landis (1996),

$$\text{TOC}\,(\%) = 67\frac{\rho_k(\rho_i - \rho)}{\rho(\rho_i - \rho_k)}, \tag{21}$$

where TOC accounts for approximately 67% of the bulk kerogen. Figure 1 shows the best fit to the experimental data, which was obtained with $\rho_i = 2.77$ g/cm^3 and $\rho_k = 1.4$ g/cm^3. Because the clays are distributed in a lenticular textural pattern, we assume that only the stiffnesses "parallel to bedding" are affected. Following Vernik (1992), we modify the stiffnesses c_{11} and c_{66} as

$$c_{11} \to \langle c_{11}\rangle, \qquad c_{66} \to \langle c_{66}\rangle, \tag{22}$$

which incorporate the respective local constants of both illite and kerogen. Figure 2 shows the phase velocities and anisotropy parameters as a function of kerogen content. As can be appreciated, the model provides a fairly good fit to the experimental values. The data show that the shale is substantially anisotropic, with positive ϵ_R and γ_R, which is characteristic of laminar transversely isotropic composites. Maximum stiffness anisotropy is obtained for a kerogen content of approximately 30%. Note that Thomsen's coefficients relate to the stiffness anisotropy and not the velocity anisotropy, which is generally lower than the stiffness anisotropy.

After we have adjusted the model to the experimental data, it is possible to analyze the anisotropic dissipation characteristics of the source rock versus kerogen content. The equivalent anisotropic parameters and quality factors for the immature shale are represented in Figure 3. The quality factor at 90°, corresponding to the horizontally polarized shear wave, is dominated by the illite dissipation, and the (rapidly decreasing) quality factor at 0° is dominated by the kerogen dissipation. As can be appreciated in Figure 3c, maximum attenuation anisotropy is obtained for a kerogen content of approximately 18%, compared with 30% for stiffness anisotropy. This is consistent with equation (19) and the fact that $c^*_{33\,\text{Im}} < c^*_{11\,\text{Im}}$.

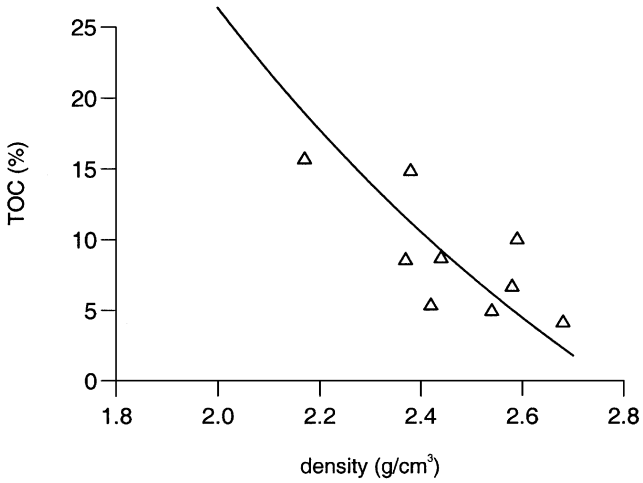

FIG. 1. Source-rock density versus total organic carbon (TOC) for samples of Kimmeridge Shale. Equation (21) is used to fit the experimental data and to obtain the kerogen and illite densities.

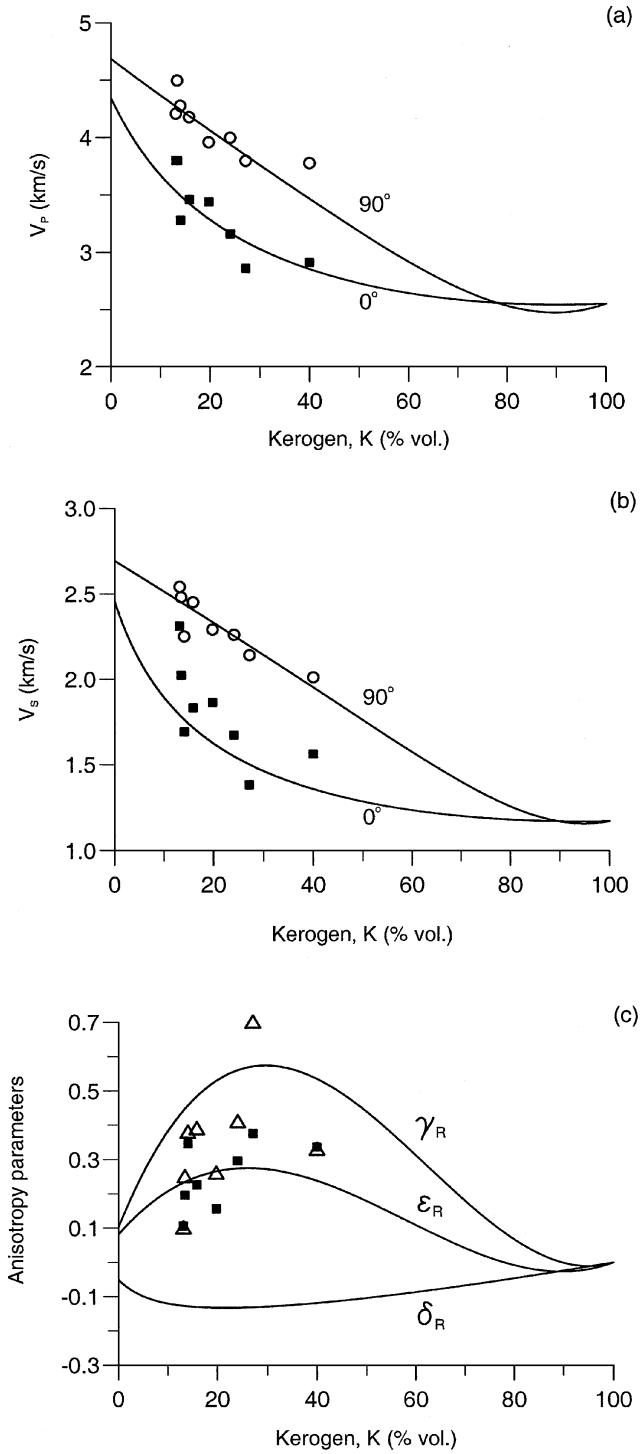

FIG. 2. Bedding-normal (0°) velocities (squares) and bedding-parallel (90°) velocities (open circles) for the compressional (a) and shear (b) waves, and Thomsen's anisotropy parameters (c) versus kerogen content for the North Sea Kimmeridge Shale. In (c), the triangles correspond to γ_R and the squares to ϵ_R. The best fit of these experimental data defines the properties of illite and kerogen, shown in Table 1.

Thus, in the range of the experimental kerogen saturations (see Figure 2), attenuation anisotropy can be an important indicator of the presence of kerogen, with shear-wave anisotropy γ_I greater than 2.

The energy velocity and the dissipation factors versus the propagation direction are displayed in Figure 4 [see Carcione

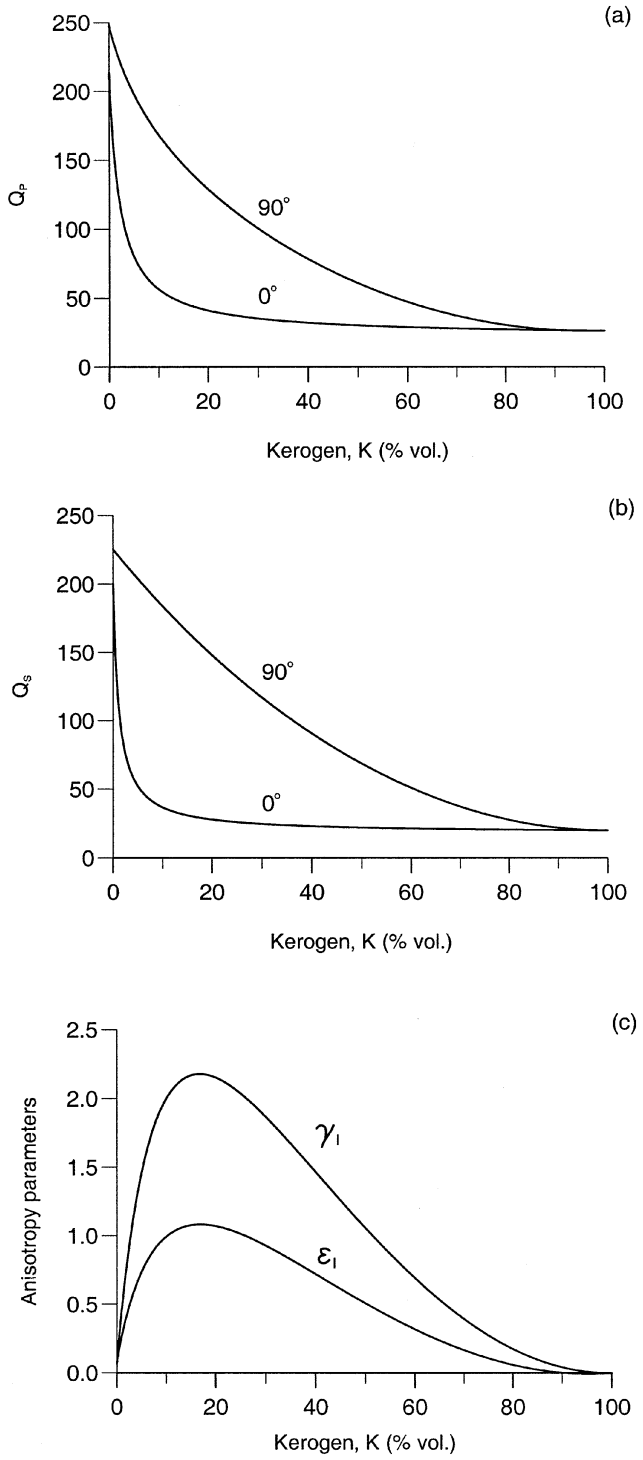

FIG. 3. Bedding-normal (0°) quality factors and bedding-parallel (90°) quality factors for the compressional (a) and shear (b) waves, and Thomsen's anisotropy parameters (c) versus kerogen content for the North Sea Kimmeridge Shale.

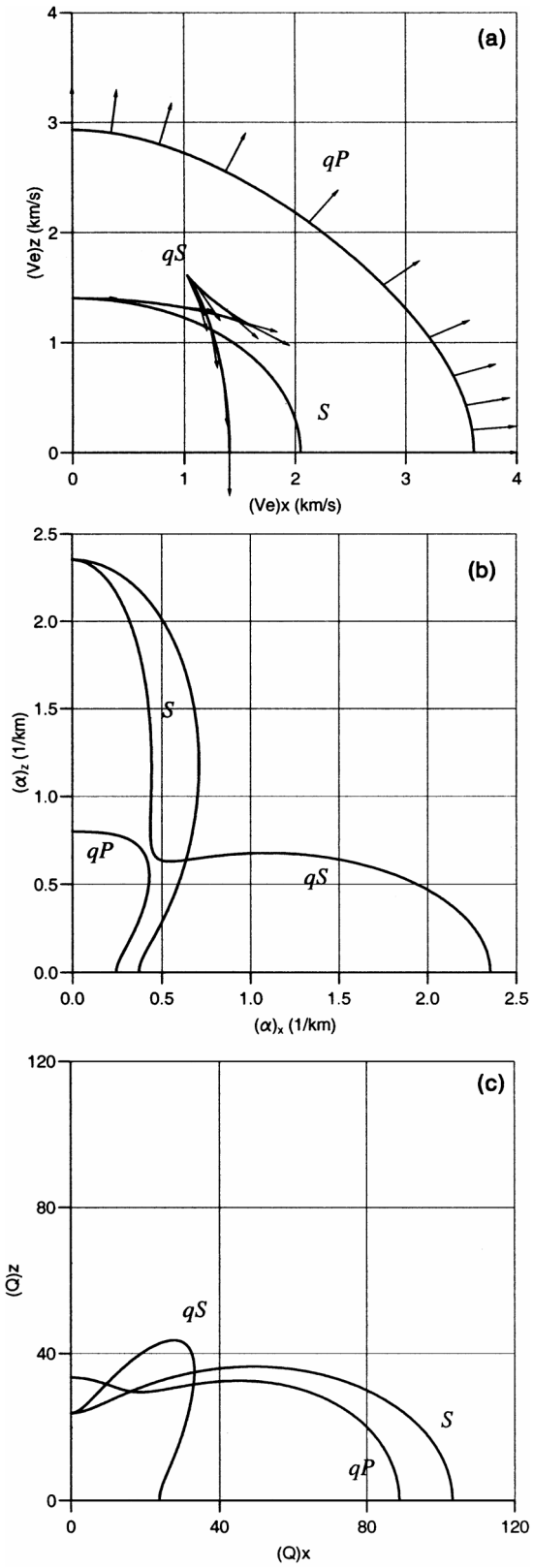

FIG. 4. Polar representation of the energy velocity (a), attenuation factor (b), and quality factor (c) for an immature source rock with 35% kerogen content. The symbols indicate the different wave modes, with qP the quasi-compressional wave, qS the quasi-shear wave, and S the antiplane shear wave. The polarizations are plotted on each curve.

(1992) for the expression of the energy velocity]. The curves correspond to 35% kerogen content. As can be seen, the dissipation shows stronger anisotropy characteristics than the wave velocities, with the *qS* curve having a more pronounced anisotropy than the *qP*- and *S*-waves for offsets ranging from 0° to 45°.

From immature to mature source rock

The different maturation stages of a source rock can be modeled by evaluating the kerogen/oil conversion and the excess pore pressure. Using certain major assumptions, discussed in detail by Berg and Gangi (1999), we can describe this relation by a simple equation, as obtained in Appendix A [equation (A-7)]. Knowing the fraction of kerogen converted to oil, we compute the properties of the kerogen/oil mixture by using the model of Kuster and Toksöz (1974) and then the properties of source rock as a function of the excess pore pressure from equation (1) (see Appendix A).

The marine Kimmeridge Shale of the Draupne Formation is located between 3480 and 3580 m in the central Viking Graben of the North Sea. The sonic log is displayed in Figure 5, along with TOC values obtained from resistivity measurements. The lithostatic pressure at a depth of $z = 3.5$ km, for an average density of $\bar{\rho} = 2.4$ g/cm^{-3}, is equal to $\bar{\rho} g z \simeq 82$ MPa, where g is the acceleration of gravity. On the other hand, the hydrostatic pore pressure is approximately 34 MPa. Thus, the maximum possible pore-pressure change Δp will be from hydrostatic to lithostatic, i.e., nearly 48 MPa (at this excess pressure, the rock may reach the fracturing stage). Under these conditions, the arguments in the exponential functions in equation (A-7) are much less than one, so these functions can be approximated by

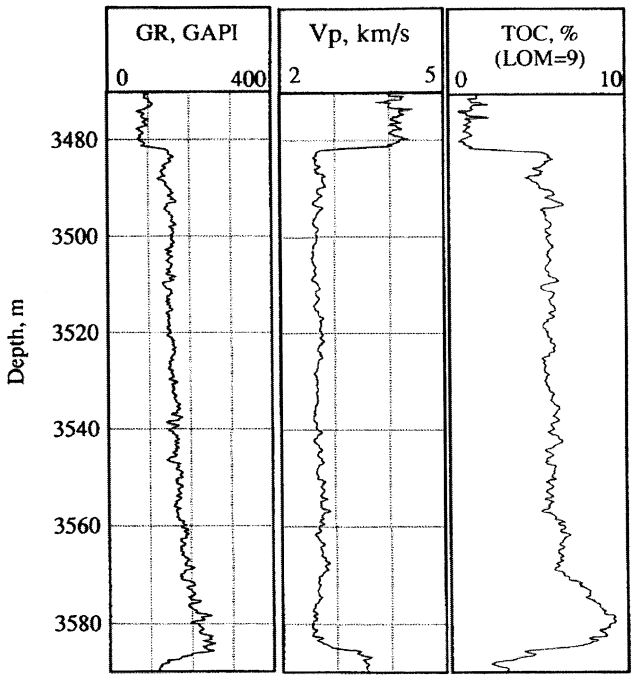

FIG. 5. Log responses of the Kimmeridge Shale, Viking Graben, North Sea.

$\exp(x) \simeq 1 + x$, $x \ll 1$, giving

$$F = \frac{(c_p + c_k)\Delta p}{D - 1 + \Delta p[c_p + c_k - D(c_p + c_o)]}, \tag{23}$$

or, more nearly correct from the physical point of view,

$$\Delta p = \frac{(D-1)F}{c_p + c_k - F[c_p + c_k - D(c_p + c_o)]}. \tag{24}$$

Equation (23) should not be misinterpreted; the effect of pressure on the kerogen oil conversion is negligible. It is the conversion of kerogen to oil that generates overpressure. Pore-space compressibilities range from $c_p = 4.2 \times 10^{-4}$/MPa (3×10^{-6}/psi, rigid rock) to $c_p = 42 \times 10^{-4}$/MPa (30×10^{-6}/psi, compliant rock), which correspond to incompressibilities of 2381 and 238 MPa, respectively. These values are in the range commonly measured for various types of rock (e.g., Fatt, 1958). On the other hand, overpressured formations have higher temperatures than the surrounding rocks (Lewis and Rose, 1970). For a thermal gradient of 25°C/km, a normally pressured Kimmeridge Shale has a temperature of about 107°C. If we assume an increase of 1.4 MPa per °C (Lewis and Rose, 1970), an excess pore pressure of 50 MPa corresponds to a formation temperature of nearly 143°C.

Equation (23) can be used for excess pressures satisfying $F \leq 1$,

$$\Delta p \leq \frac{D-1}{D(c_p + c_o)},$$

and finite pore-space compressibilities. As the porosity decreases, the pore-space stiffness generally decreases, and therefore, c_p increases. Following Mavko and Mukerji (1995) and neglecting the mineral-grain compressibility [see equation (8) in Zimmerman et al., 1986], we consider that the pore-space stiffness c_p^{-1} decreases linearly with porosity (kerogen content). We assume

$$c_p[\text{MPa}^{-1}] = (2381 - 5357\ \text{K})^{-1}, \tag{25}$$

such that the pore incompressibility lies between the lower and upper limits mentioned above—2381 MPa for $\text{K} \approx 0$, and 238 for $\text{K} = 0.4$. As for sandstones, equation (25) is based on the "critical-porosity" concept. The critical porosity K_c separates load-bearing sediments from suspensions (Nur, 1992) (in this case, $\text{K}_c \approx 0.44$ for $c_p = \infty$). According to equation (25), a Kimmeridge Shale with 35% kerogen content has a pore stiffness of 506 MPa.

Figure 6 represents the fraction of kerogen converted to oil (a) and the porosity (b) versus excess pore pressure, for different pore-space compressibilities. The curves labeled "Kimmeridge" are computed with an initial kerogen content of 35%. At the same value of the conversion factor, the excess pore pressure is higher for rigid rocks than for compliant rocks. For this simulation of the Kimmeridge Shale, the effective pressure necessary to reach fracture is 48 MPa, with about 28% of the kerogen converted to oil. At this pressure, the porosity increase is approximately 10% of the initial porosity.

The kerogen/oil conversion versus the initial kerogen content is shown in Figure 7, for an excess pressure of 30 MPa. The curve increases from the value for a rigid rock (we assumed a finite compressibility at $\text{K} \approx 0$) to the value corresponding to a

compliant rock (see Figure 6a). Bedding-normal (0°) velocities, bedding-parallel (90°) velocities, and Thomsen's anisotropy parameters (c) versus initial kerogen content are shown in Figure 8. The pore-space compressibility is given by equation (25), and the excess pore pressure is 30 MPa. Compared to the case $\Delta p = 0$ MPa (Figure 2), there is an important velocity decrease, mainly at 0°, beyond K ≈ 10%. This implies higher anisotropy parameters at high kerogen content, as can be appreciated in Figure 8c. The corresponding quality factors and anisotropy parameters are represented in Figure 9. Compared with Figure 3, quality factors perpendicular to layering decrease and quality factors parallel to layer increase slightly with initial kerogen

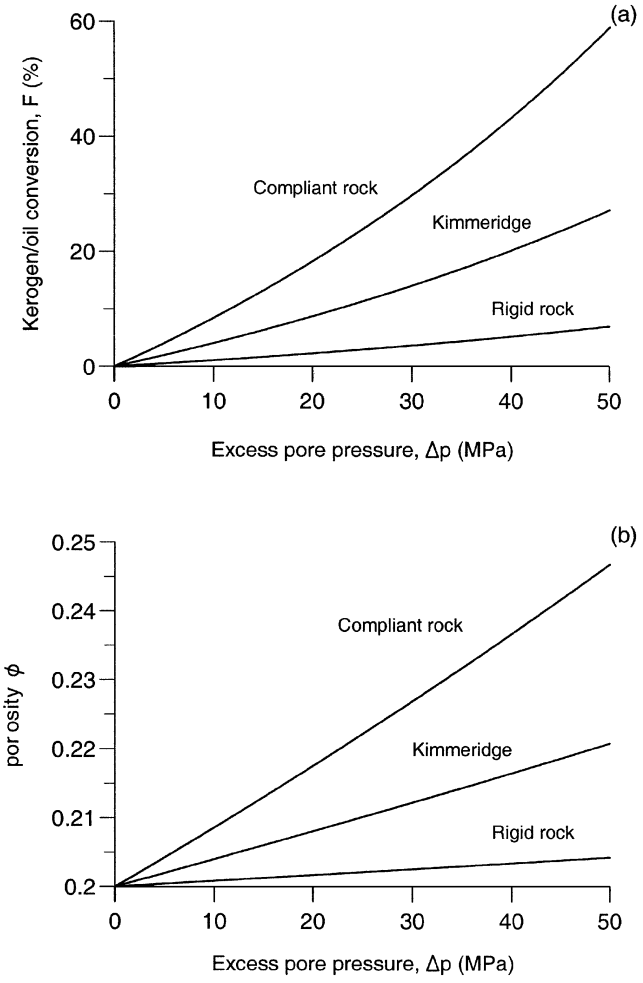

FIG. 6. Fraction of kerogen converted to oil (a) and porosity (b) versus excess pore pressure. The calculation assumes an initial kerogen content of 35%.

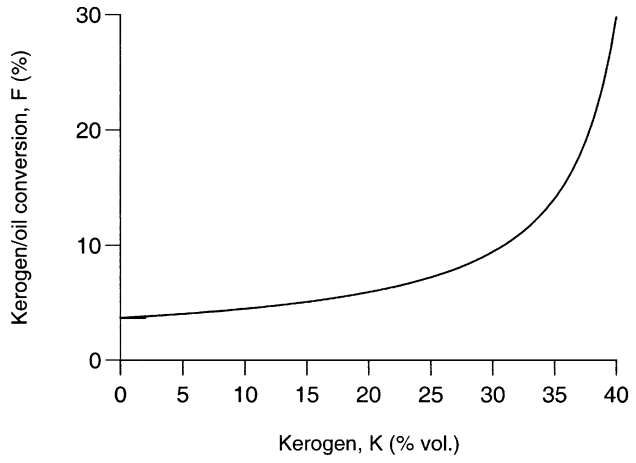

FIG. 7. Kerogen-to-oil conversion at an excess pore pressure of 30 MPa versus the initial convertible kerogen.

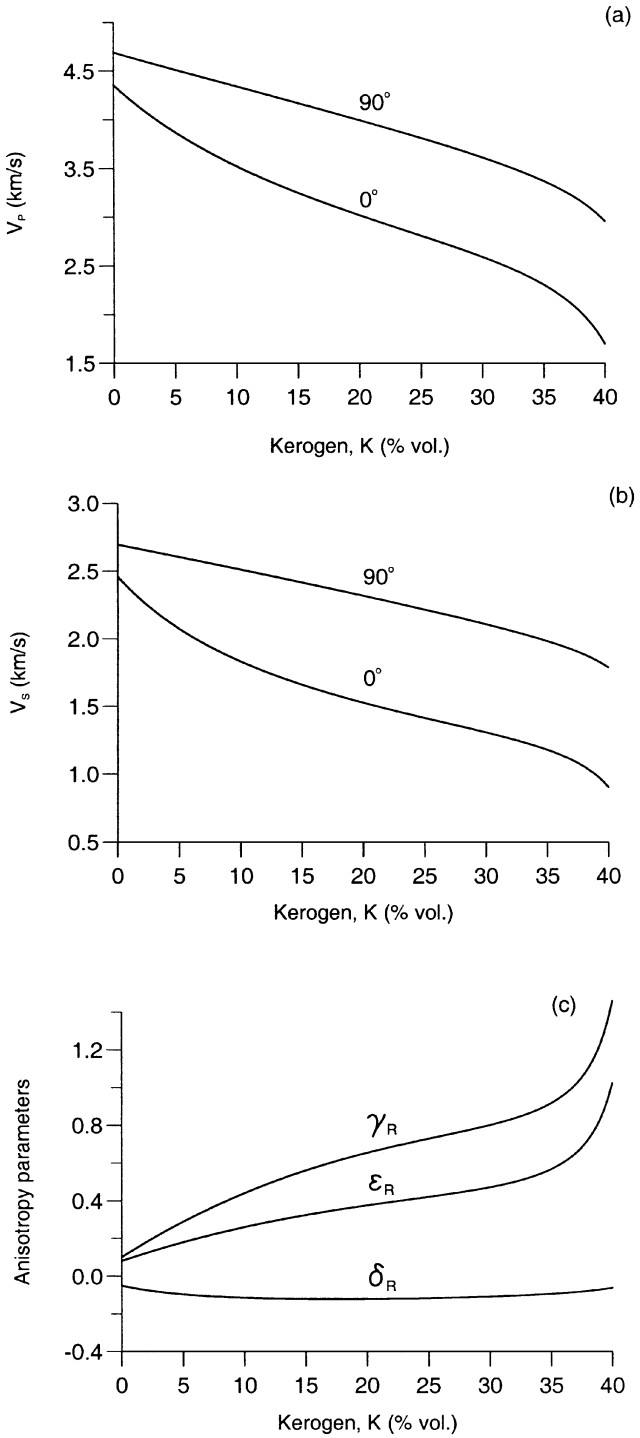

FIG. 8. Bedding-normal (0°) velocities and bedding-parallel (90°) velocities for the compressional (a) and shear (b) waves, and Thomsen's anisotropy parameters (c) versus initial kerogen content. The excess pore pressure is 30 MPa.

content (the cause of this behavior is explained below). The kerogen/oil conversion increases the anisotropy in attenuation for high initial kerogen content.

Wave velocities and anisotropy parameters versus excess pore pressure are represented in Figure 10, where an initial kerogen content of 35% has been assumed. The bedding-normal velocities decrease more rapidly than the parallel velocities, implying higher anisotropy parameters with increasing pore pressure. The quality factors, represented in Figure 11, show a different behavior; $Q(0^\circ)$ decreases for both waves and $Q(90^\circ)$ increases with pore pressure, causing a significant attenuation anisotropy at high pressures. The fact that $Q(90^\circ)$ increases for lower Qs of the kerogen/oil mixture is paradoxical.

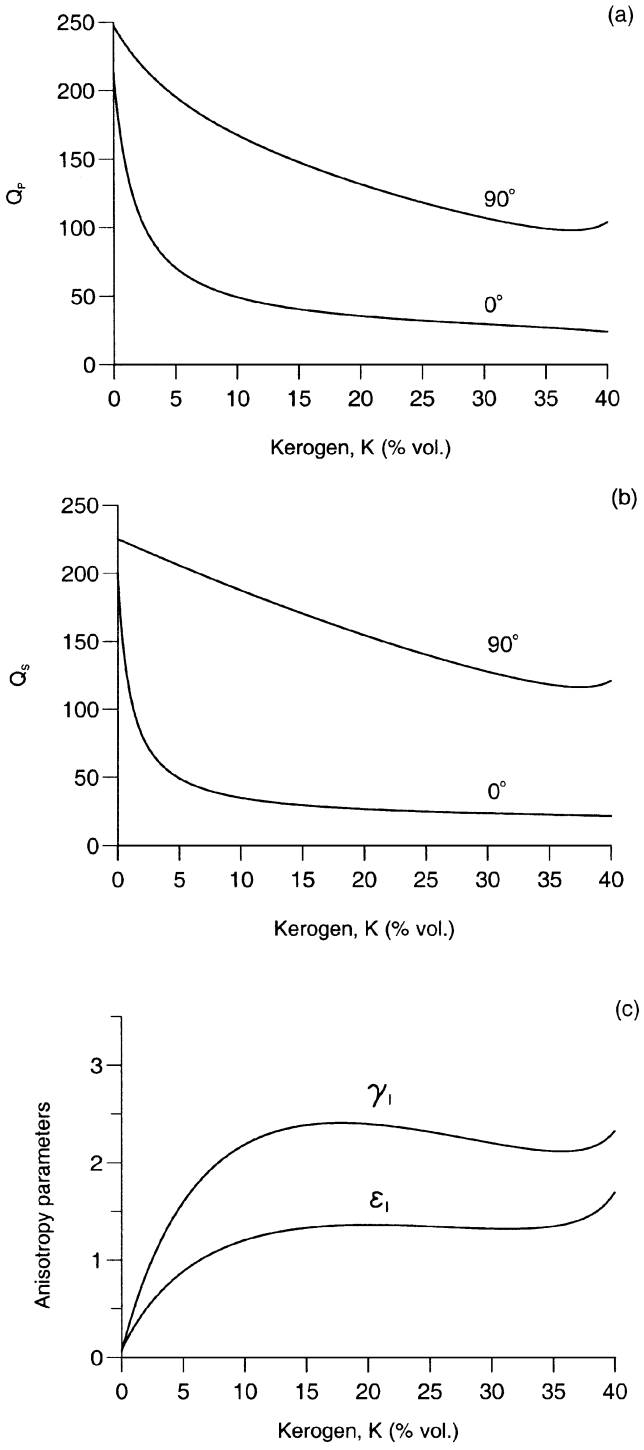

FIG. 9. Bedding-normal (0°) quality factors and bedding-parallel (90°) quality factors for the compressional (a) and shear (b) waves, and Thomsen's anisotropy parameters (c) versus kerogen content. The excess pore pressure is 30 MPa.

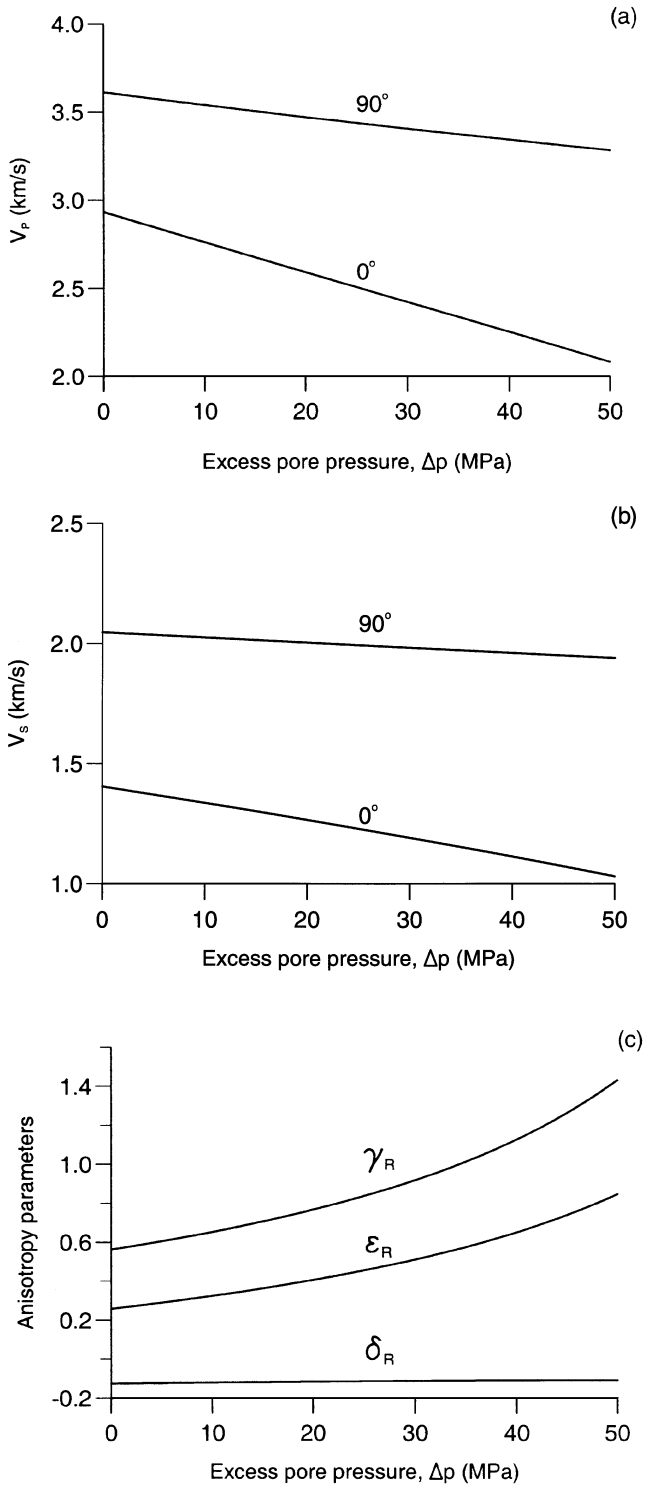

FIG. 10. Bedding-normal (0°) velocities and bedding-parallel (90°) velocities for the compressional (a) and shear (b) waves, and Thomsen's anisotropy parameters (c) versus excess pore pressure, for an initial kerogen content of 35%.

To examine this, let us consider, for simplicity, the quality factor of the *S*-wave. From the last equation (1) and equation (20) and after some calculation, we obtain

$$Q_{66} = \left[1 + \frac{C}{c_{66}^{(m)}}\right] Q_m, \qquad C = \frac{(1-\mathrm{K})^2}{\mathrm{K}(2-\mathrm{K})} c_{66}^{(i)},$$

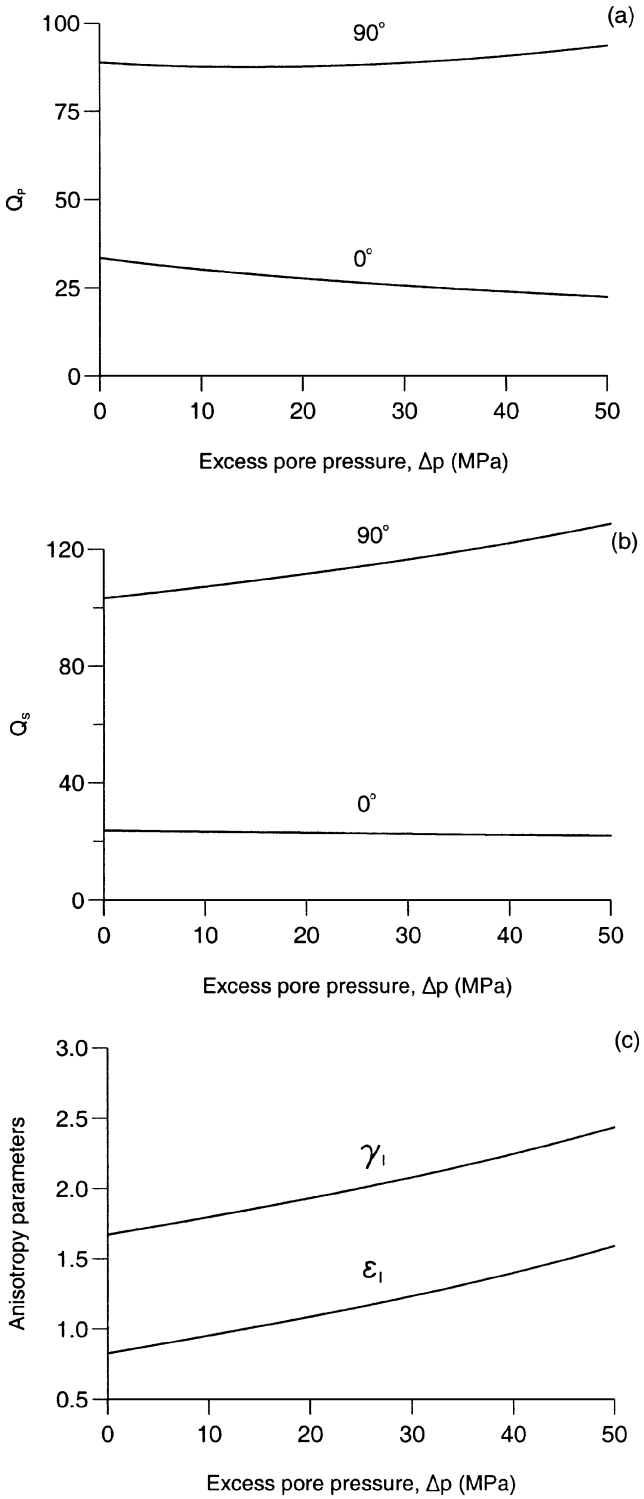

FIG. 11. Bedding-normal (0°) quality factors and bedding-parallel (90°) quality factors for the compressional (a) and shear (b) waves, and Thomsen's anisotropy parameters (c) versus excess pore pressure, for an initial kerogen content of 35%.

where $c_{66}^{(i)}$ is the illite stiffness, $c_{66}^{(m)} = c_{55}^{(m)}$ is the stiffness of the kerogen/oil mixture, computed with the theory of Kuster and Toksöz (1974) (see Appendix A), and $Q_m = c_{66\mathrm{R}}^{(m)}/c_{66\mathrm{Im}}^{(m)}$. Like the quality factor, the stiffness of the mixture $c_{66}^{(m)}$ decreases with increasing pore pressure. In this case, $c_{66}^{(m)}$ decreases faster than Q_m; therefore, Q_{66} increases with pore pressure. Polar representations of the energy velocity (a), attenuation factor (b), and quality factor (c) for 35% kerogen content and an excess pore pressure of 30 MPa are displayed in Figure 12. The anisotropy is more pronounced with respect to the case $\Delta p = 0$, represented in Figure 4. This can be appreciated by comparing the cuspidal triangles of the *qSV*-waves and the quality-factor curves.

In the area investigated (see Figure 5), the chalk/source rock interface at 3480-m depth yields a strong seismic reflection because of the high impedance contrast. An estimation of the impedance contrasts can be obtained from the inversion of zero-offset stacked sections. A rough estimation of the normalized *P*-wave impedance contrasts can be calculated from

$$R_{II} = \frac{Z - Z_{II}}{Z + Z_{II}}, \quad Z_{11} = \rho V_{ph}(90^\circ), \quad Z_{33} = \rho V_{ph}(0^\circ), \tag{26}$$

where Z is the impedance of the isotropic chalk (repeated indices do not imply implicit summation). Figure 13 represents R_{II} versus kerogen content at $\Delta p = 0$ MPa (a) and excess pore pressure for $\mathrm{K} = 35\%$ (b). The chalk *P*-wave acoustic impedance is $Z = 13.34 \times 10^6$ kg m^{-2} s^{-1}, corresponding to a velocity of 4600 m/s and a density of 2900 kg/m^3 (see Figure 5). The impedance contrast computed with the velocities normal to the stratification (R_{33}) is higher than that parallel to it (R_{11}). Note that bedding-normal impedances are obtained, for instance, from well profiles such as sonic and density logs, and bedding-parallel velocities are obtained from seismic inversion of reflection data. As expected, augmenting kerogen content and pore pressure increases the seismic visibility of the shale.

Finally, we compute the compressional- and shear-wave velocities versus excess pore pressure, including water in the pore space. They are shown in Figure 14, where the continuous lines correspond to the bedding-parallel velocities and the broken lines to the bedding-normal velocities (the equation for F as a function of the initial water saturation S_{wi} is given in Appendix A). The figures indicate that the bedding-normal velocities are affected greatly by water content.

CONCLUSIONS

The characteristics of the wave velocities, attenuation factors, quality factors, and stiffness and attenuation anisotropy parameters versus kerogen content and excess pore pressure provide a diagnostic approach for predicting kerogen content and maturation level from seismic data. This study demonstrates that anisotropy of wave velocity and attenuation are linked strongly to kerogen content and maturation. Inversely, velocity and attenuation may be used as indicators for the detection of kerogen-rich shales having different maturation levels. These levels depend on the pressure change resulting from oil generation in low-permeability source rocks. From the North Sea Kimmeridge Shale properties, we conclude:

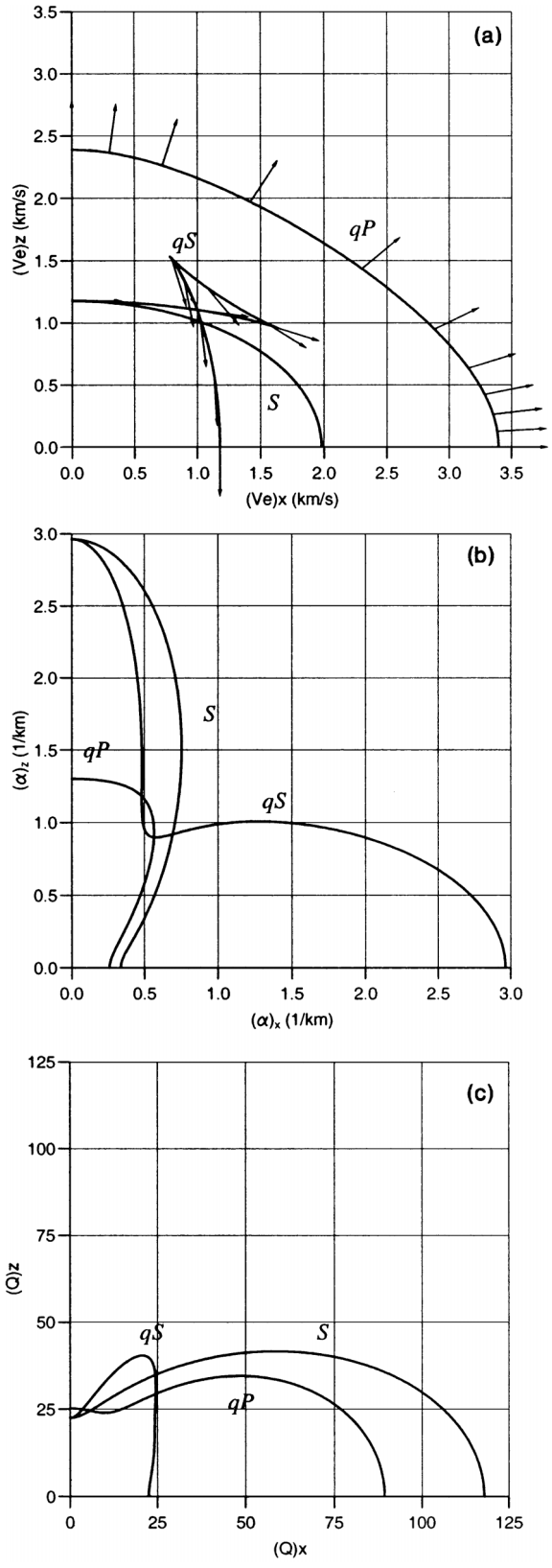

FIG. 12. Polar representation of the energy velocity (a), attenuation factor (b), and quality factor (c) for a source rock with 35% kerogen content and subject to an excess pore pressure of 30 MPa. The symbols indicate the different wave modes, with qP the quasi-compressional wave, qS the quasi-shear wave, and S the antiplane shear wave. The polarizations are plotted on each curve.

1) For immature source rocks (assumed to be normally pressured), the generalized Thomsen's anisotropy parameters ϵ_R and γ_R are positive, and maximum anisotropy is obtained for a kerogen content of about 30%.
2) Normal-bedding quality factors are lower than parallel-bedding quality factors and decrease rapidly with kerogen content less than 20%. Attenuation anisotropy is higher than stiffness anisotropy with maximum values at about 18%. Attenuation anisotropy of the qS-wave versus propagation direction is stronger than the anisotropy of the qP- and S-waves.
3) Kerogen-to-oil conversion produces excess pore pressure. This process simulates the different maturation levels. At the same value of the conversion factor, the excess pressure is higher in rigid rocks. For instance, for a Kimmeridge Shale with 35% kerogen content, the pore pressure necessary to reach fracture is 48 MPa, with about 28% of the kerogen converted to oil. At this pressure, the porosity increase is approximately 10% of the initial porosity.
4) The anisotropy parameters increase and the velocities decrease with increasing kerogen-to-oil conversion and

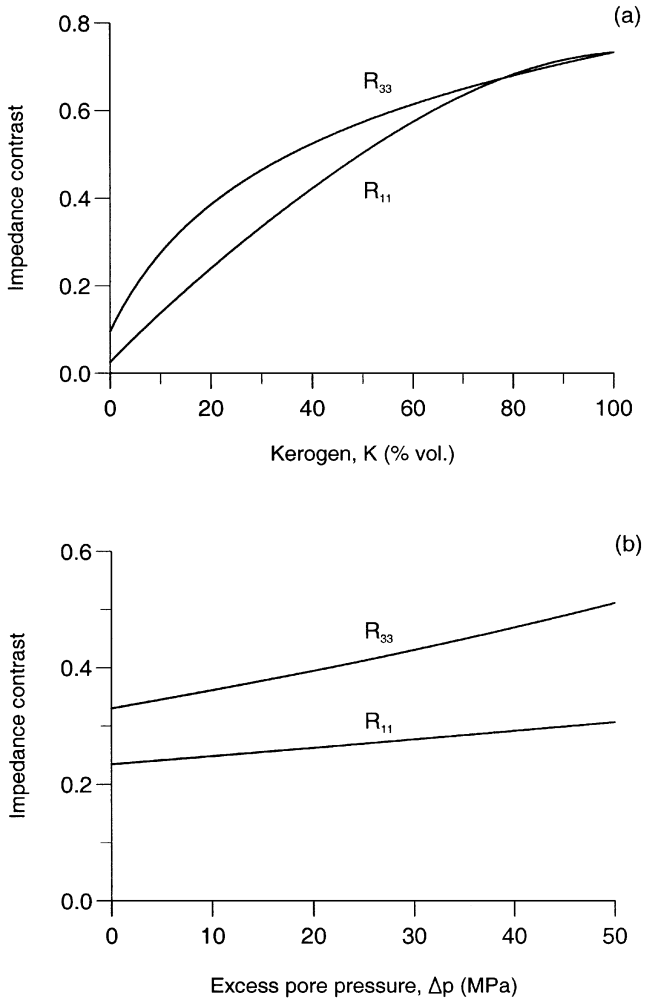

FIG. 13. P-wave impedance contrasts between a chalk overlying a hydrocarbon source rock (a) versus kerogen content at $\Delta p = 0$ MPa and (b) versus excess pore pressure for an initial kerogen content K = 35%.

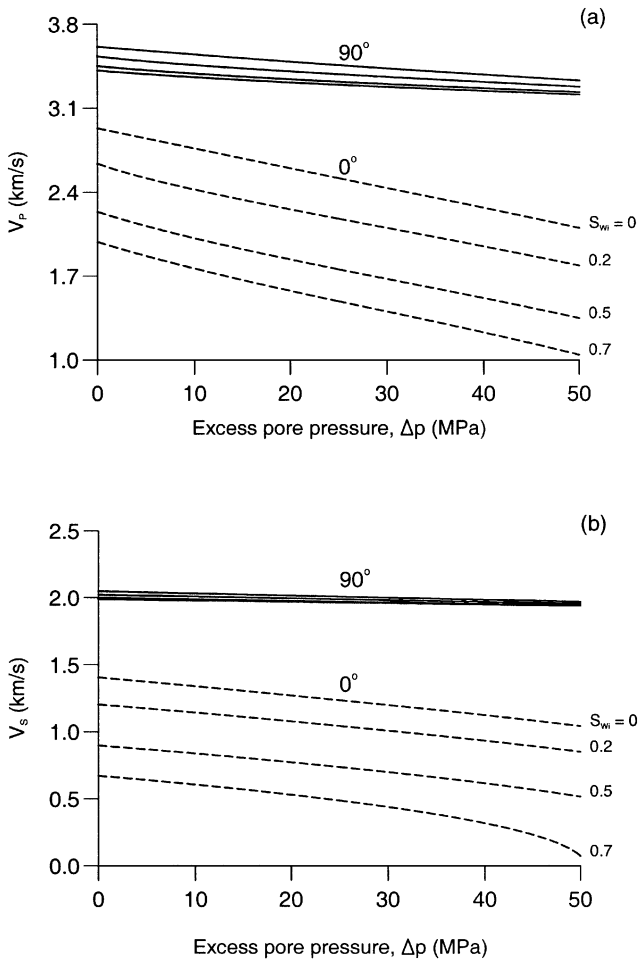

FIG. 14. Bedding-normal (0°) velocities and bedding-parallel (90°) velocities for the compressional (a) and shear (b) waves, for an initial kerogen content of 35% and several initial water saturations.

excess pore pressure. Normal-bedding quality factors decrease, but parallel quality factors increase slightly with kerogen content.

5) The polar anisotropy, i.e., variations with respect to the propagation direction, is more pronounced at high pore pressures and conversion factors.
6) Augmenting kerogen content and pore pressure increases the seismic visibility of the shale. The impedance contrasts calculated with the bedding-normal velocities are more sensitive than those computed with the parallel-bedding velocities.
7) Water saturation greatly affects the bedding-normal velocities.

Extension of this investigation to a more realistic situation should consider the conversion of oil to gas. Moreover, it is known that pore-volume compressibility increases greatly as the pore pressure approaches the fracture pressure (Zimmerman et al., 1986). The role of temperature is also important. For instance, there is experimental evidence that the ratio of compressional to shear velocity increases with temperature when measured in the direction normal to bedding (Vernik and Nur, 1992).

ACKNOWLEDGMENTS

This work was supported by Norsk Hydro a.s. (Bergen) with funds of the "Source Rock" project and by the European Union under the project "Detection of overpressure zones with seismic and well data." Thanks to Hans B. Helle, Michael Batzle, and an anonymous reviewer for important technical comments.

REFERENCES

Ben-Menahem, A., and Singh, S. G., 1981, Seismic waves and sources, Springer-Verlag, Berlin.
Berg, R. R., and Gangi, A. F., 1999, Primary migration by oil-generation microfracturing in low-permeability source rocks: Application to the Austin chalk, Texas: AAPG Bull., **83**, no. 5, 727–756.
Carcione, J. M., 1992, Anisotropic *Q* and velocity dispersion of finely layered media: Geophys. Prosp., **40**, 761–783.
Carcione, J. M., Cavallini, F., and Helbig, K., 1998, Anisotropic attenuation and material symmetry: Acustica, **84**, 495–502.
Fatt, I., 1958, Pore volume compressibilities of sandstone reservoir rocks: AIME Petr. Trans., **213**, 362–364.
Hauge, P. S., 1981, Measurements of attenuation from vertical seismic profiles: Geophysics, **46**, 1548–1558.
Johnston, D. H., 1987, Physical properties of shale at temperature and pressure: Geophysics, **52**, 1391–1401.
Kuster, G. T., and Toksöz, M. N., 1974, Velocity and attenuation of seismic waves in two-phase media, Part I: Theoretical formulations: Geophysics, **39**, 587–606.
Lewis, C. R., and Rose, S. C., 1970, A theory relating high temperatures and overpressure: J. Petr. Tech., **22**, 11–16.
Mavko, G., and Mukerji, T., 1995, Seismic pore space compressibility and Gassmann's relation: Geophysics, **60**, 1743–1749.
McCain, W. D. Jr., 1984, The properties of petroleum fluids: Penn Well Publ. Co.
Meissner, F. F., 1978, Petroleum geology of the Bakken Formation, Williston Basin, North Dakota and Montana: Montana Geol. Soc. Symp., 207–227.
Nur, A., 1992, Critical porosity and the seismic velocities in rocks: EOS, **73**, 43–66.
Schoenberg, M., and Muir, F., 1989, A calculus for finely layered media: Geophysics, **54**, 582–590.
Thomsen, L., 1986, Weak elastic anisotropy: Geophysics, **51**, 1954–1966.
Todd, T., and Simmons, G., 1972, Effect of pore pressure on the velocity of compressional waves in low-porosity rocks: J. Geophys. Res., **77**, 3731–3743.
Toksöz, M. N., and Johnston, D. H., Eds., 1981, Seismic wave attenuation: Soc. Expl. Geophys.
Vernik, L., 1994, Hydrocarbon-generation-induced microcraking of source rocks: Geophysics, **59**, 555–563.
Vernik, L., and Landis, C., 1996, Elastic anisotropy of source rocks: Implications for hydrocarbon generation and primary migration: AAPG Bull., **80**, 531–544.
Vernik, L., and Nur, A., 1992, Ultrasonic velocity and anisotropy of hydrocarbon source rocks: Geophysics, **57**, 727–735.
Zimmerman, R. W., Somerton, W. H., and King, M. S., 1986, Compressibility of porous rocks: J. Geophys. Res., **91**, 12765–12777.
Zimmerman, R. W., 1991, Compressibility of sandstones: Elsevier Science Publ. Co., Inc.

APPENDIX A

EXCESS PORE PRESSURE, POROSITY, AND ORGANIC-MATTER PROPERTIES

Kerogen-to-oil conversion versus excess pressure

The petrophysical characteristics of the source rock and the hydrocarbon generation process are those illustrated first by Meissner (1978) and more recently by Vernik (1994). Anomalous fluid pressures are developed by conversion of kerogen to oil. After the pore pressure exceeds the overburden pressure, the rock fractures and the generated oil is expelled as a continuous porosity-saturating phase through an oil-wet rock matrix.

In fact, excess pore pressure (overpressuring) is believed to be the main mechanism for oil migration. This phenomenon occurs mainly in low-permeability rocks (e.g., compacted shales), where high-density organic matter, such as kerogen, is transformed to less dense fluids (oil and gas), with a rate exceeding the rate of volume loss by flow. To obtain a simple formula for computing the excess pore pressure as a function of the volume fraction of kerogen transformed to oil, we follow the approach given in Berg and Gangi (1999). The following assumptions are made: 1) no fluid is lost from the source-rock pore volume (negligible permeability); 2) the rock compressibilities are independent of pressure and temperature; 3) the initial pore volume contains only convertible kerogen, because water content is very small and is part of the matrix (smectite); 4) conversion of oil to gas is negligibile; 5) the confining pressure is approximately constant during oil generation, i.e., the reaction rate is high enough that the overburden pressure does not change significantly during the conversion process; and 6) volume changes with temperature are negligible.

Let us define the excess pore pressure by $\Delta p = p - p_{\mathrm{i}}$, where p_{i} is the initial pore pressure and p is the pore pressure when a fraction F of kerogen mass has been converted to oil. The excess pore pressure is equal to the difference in effective pressure Δp_e divided by the effective stress coefficient n, because the confining pressure p_c is assumed constant at a given depth. We recall that $p_e = p_c - np$ (Todd and Simmons, 1972).

Because the mass balance is independent of pressure, the amount of converted oil can be expressed as

$$\rho_o V_{\mathrm{oi}} = F \rho_k V_{\mathrm{ki}}, \tag{A-1}$$

where ρ_o is the oil density and V_{oi} and V_{ki} are the oil and kerogen volumes at p_{i}, respectively. The pore volume at the initial pore pressure is $V_{p\mathrm{i}} = V_{\mathrm{ki}}$ because there is only kerogen.

The (unrelaxed) compressibilities of the oil, kerogen, and pore space are defined, respectively, as

$$c_o = -\frac{1}{V_o}\frac{dV_o}{dp}, \qquad c_k = -\frac{1}{V_k}\frac{dV_k}{dp}, \qquad c_p = +\frac{1}{V_p}\frac{dV_p}{dp}. \tag{A-2}$$

Note that $c_o = (\rho_o V_{11}^2)^{-1}$ and $c_k = (\hat{c}_{13} + 2\hat{c}_{55}/3)^{-1}$, where $\hat{c}_{IJ} = \rho V_{IJ}^2$, with V_{IJ} of each medium given in Table 1. The plus sign means that the pore volume increases with increasing pore pressure (see Figure A-1), since c_p is the compressibility at constant confining pressure (Zimmerman, 1991). Integration from p to p_{i} yields

$$V_o(p) = V_{\mathrm{oi}} \exp(-c_o \Delta p), \qquad V_k(p) = V_{\mathrm{ki}} \exp(-c_k \Delta p), \tag{A-3}$$
$$V_p(p) = V_{\mathrm{ki}} \exp(c_p \Delta p).$$

Using (A-1), the oil volume becomes

$$V_o(p) = FDV_{\mathrm{ki}} \exp(-c_o \Delta p), \tag{A-4}$$

where $D = \rho_k/\rho_o$. Because the pore-space volume at pressure p is

$$V_p = (1 - F)V_k + V_o, \tag{A-5}$$

we obtain

$$\exp(c_p \Delta p) = (1 - F)\exp(-c_k \Delta p) + FD \exp(-c_o \Delta p). \tag{A-6}$$

Finally, the fraction of kerogen converted to oil can be expressed as

$$F = \frac{1 - \exp[-(c_p + c_k)\Delta p]}{D \exp[-(c_p + c_o)\Delta p] - \exp[-(c_p + c_k)\Delta p]}. \tag{A-7}$$

For $\Delta p \to 0$, $F \to 0$, and for $\Delta p \to \infty$, $F \to 1$.

Porosity versus excess pressure

As the pore pressure increases from p_{i} to p, the pore-space volume increases from V_{ki} to $V_{\mathrm{ki}} \exp(c_p \Delta p)$ (Figure A-1).

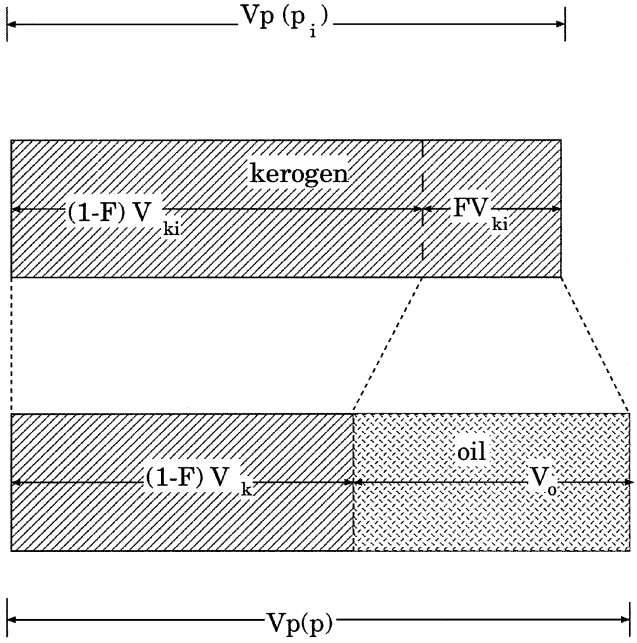

FIG. A-1. The variation of the pore, kerogen, and oil volumes with pore pressure: (a) the volume at the initial pore pressure p_{i} (before any kerogen is converted into oil), and (b) the volumes at the subsequent pore pressure p when a fraction F of kerogen has been converted to oil.

Defining the initial porosity as the kerogen proportion K, the porosity increases from this value to K $\exp(c_p\Delta p)$. Then, using equation (A-6), we can express the kerogen and oil proportions as a function of pore pressure as

$$\phi_k = \mathrm{K}(1-F)\exp(-c_k\Delta p), \quad \phi_o = \mathrm{K}FD\exp(-c_o\Delta p), \tag{A-8}$$

respectively. Defining ϕ_i as the illite proportion, we get

$$\phi_i = 1-\phi_k-\phi_o = 1-\mathrm{K}\exp(c_p\Delta p). \tag{A-9}$$

Properties of the kerogen/oil mixture

We consider that the kerogen/oil mixture consists of oil bubbles embedded in a kerogen matrix. The complex stiffness of this mixture can be calculated by using the model developed by Kuster and Toksöz (1974) for spherical inclusions. If s is the oil concentration, $s=\phi_o/(\phi_o+\phi_k)=FD\exp[-(c_p+c_o)\Delta p]$, and the stiffnesses are

$$\frac{c_{13}^{(m)}+\frac{2}{3}c_{55}^{(m)}}{K_k} = \frac{1+[4\mu_k(K_o-K_k)/(3K_o+4\mu_k)K_k]s}{1-[3(K_o-K_k)/(3K_o+4\mu_k)]s} \tag{A-10}$$

and

$$\frac{c_{55}^{(m)}}{\mu_k} = \frac{(1-s)(9K_k+8\mu_k)}{9K_k+8\mu_k+s(6K_k+12\mu_k)}, \tag{A-11}$$

where $K_k=c_{13}+2c_{55}/3$ and $\mu_k=c_{55}$, with c_{13} and c_{55} given in equation (8). Each bubble of oil is described by the complex bulk modulus

$$K_o = \rho_o V_{11}^2 M_1, \tag{A-12}$$

where V_{11} is the elastic high-frequency limit compressional velocity and M_1 is the dimensionless dilatational modulus (see Table 1). Finally, the density of the mixture is simply $(\phi_k\rho_k+\phi_o\rho_o)/(\phi_k+\phi_o)$.

Equations including water in the pore space

When the initial water saturation is S_{wi}, equation (A-7) and the oil and water saturations are

$$F = \frac{S_{wi}\exp(-c_w\Delta p)+(1-S_{wi})\exp(-c_p\Delta p)-\exp(c_p\Delta p)}{(1-S_{wi})[\exp(-c_k\Delta p)-D\exp(-c_o\Delta p)]}, \tag{A-13}$$

$$s = (1-S_{wi})FD\exp[-(c_k+c_o)\Delta p], \tag{A-14}$$

$$S_w = S_{wi}\exp[-(c_k+c_w)\Delta p]. \tag{A-15}$$

The properties of the oil/water/kerogen mixture are obtained by Wood's average of the unrelaxed oil and water compressibilities and by using Kuster and Töksoz's equations and substituting s by $s+S_{wi}$ in equations (A-10) and (A-11).